Structural Characterization of Molybdenum Oxide Supported on Zirconia

Shuibo Xie, Kaidong Chen, Alexis T. Bell,* and Enrique Iglesia*

Chemical and Materials Sciences Divisions, E. O. Lawrence Berkeley National Laboratory, and Department of Chemical Engineering, University of California, Berkeley, California 94720-1462

Received: July 6, 2000

X-ray diffraction and X-ray absorption and Raman spectroscopies were used to determine the structure of dispersed and crystalline structures in MoO_x/ZrO_2 catalysts useful in the oxidative dehydrogenation of alkanes. The MoO_x surface density on ZrO_2 was varied over a wide range (0.35−50 Mo/nm^2) by changing the Mo content (1−44 wt % MoO_3) and the treatment temperature (393−973 K). Raman spectra showed that MoO_x/ZrO_2 samples with low surface density (<5 Mo/nm^2) treated at temperatures below 873 K initially contain isolated tetrahedral MoO_x species; these species oligomerize to form two-dimensional structures with bridging Mo−O−Mo bonds as the surface density increased to values typical for a polymolybdate monolayer (∼5 Mo/nm^2). An increase in surface density led to a shift in the ν(Mo═O) Raman band to higher frequencies and to changes in the near-edge X-ray absorption spectra. Both of these are consistent with the growth of these polymolybdate domains with increasing Mo surface density, as also suggested by the concurrent decrease in the UV−visible absorption energy. Thermal treatment at 973 K led to the dissociation of Mo−O−Mo bonds and to the formation of tetragonal−pyramidal O═MoO_4 species. For MoO_x/ZrO_2 samples with Mo surface densities greater than 5 Mo/nm^2, MoO_3 and $Zr(MoO_4)_2$ were detected by Raman and for larger crystallites also by X-ray diffraction. Treatment of these samples in air at 723 K led to the predominant formation of MoO_3, while higher temperatures led to a solid-state reaction between MoO_3 and ZrO_2 to form $Zr(MoO_4)_2$. This structural evolution was confirmed by the evolution of pre-edge and near edge features in the X-ray absorption spectra of these high surface density samples. $Zr(MoO_4)_2$ contains Mo^{6+} cations in a distorted tetrahedral coordination with one oxygen bonded only to molybdenum and the other three shared by Zr and Mo atoms. The Raman bands observed for $Zr(MoO_4)_2$ at 750, 945, and 1003 cm^{-1} were assigned to ν_{sym}(O−Mo−O), ν_{asym}(O−Mo−O), and ν(Mo═O) vibrational modes, respectively, based on the analysis of the Raman bands observed after $^{18}O_2$ exchange with lattice oxygen atoms. Bridging O atoms in Mo−O−Mo species exchanged with gas phase $^{18}O_2$ more readily than terminal Mo═O species.

Introduction

The thermodynamic feasibility of oxidative dehydrogenation (ODH) of alkanes has led to extensive evaluation of oxide catalysts for these reactions. Supported vanadium and molybdenum oxides have been widely used for selective oxidation reactions.[1−10] Recently, propane ODH rates and selectivity on MoO_x/ZrO_2 catalysts were shown to depend strongly on the MoO_x surface density, which was varied by changing the Mo content and the catalyst treatment temperature.[11] The evolution of the structure of ZrO_2-supported molybdenum oxide from isolated MoO_x to two-dimensional oligomers and ultimately to MoO_3 or $Zr(MoO_4)_2$ bulk structures depends on the Mo surface density, the treatment temperature, and the reactivity of the support. Here, we report the details of this structural evolution. ZrO_2-supported MoO_x with Mo surface densities ranging from 0.35 to 50 Mo/nm^2 were characterized by Raman spectroscopy, X-ray diffraction, and X-ray absorption spectroscopy in order to understand how their structures evolved during catalyst synthesis and pretreatment. Raman spectroscopy probes the vibrational modes and thus the local structure and metal−oxygen bond strength in dispersed oxide domains.[12−15] X-ray absorption spectroscopy (XAS) is a direct probe of the atomic environment and it provides chemical bonding information, such as coordination numbers and interatomic distances of neighboring atoms around the absorber.[16]

Experimental Section

The syntheses of the zirconia support and of MoO_x/ZrO_2 catalysts have been reported elsewhere.[11] Hydrous zirconium oxyhydroxide, $ZrO_x(OH)_{4-2x}$, was precipitated at a pH of 10 from a 1 M aqueous solution of zirconyl chloride by controlled addition of ammonium hydroxide solutions. After precipitation, the solids were washed with mildly basic ammonium hydroxide solution (pH ∼ 8) until AgCl precipitates were no longer detected in the effluent by the dropwise addition of a 3 M $AgNO_3$ solution ($[Cl^-] < 10^{-10}$ M). The precipitated powders were dried in air overnight at 393 K. MoO_x/ZrO_2 samples were prepared by incipient wetness impregnating the $ZrO_x(OH)_{4-2x}$ powders dried at 393 K with a solution of ammonium dimolybdate (Aldrich, 99%) or ammonium heptamolybdate (Aldrich, 99%). The Mo^{6+} concentration in the impregnating solution was varied in order to achieve the desired Mo content. After impregnation, samples were dried overnight in air at 393 K and then treated in flowing dry air at 723, 773, or 873 K for 3 h before reaction and characterization measurements.

Raman spectra were recorded using a HoloLab 5000 Raman spectrometer (Kaiser Optical) equipped with a Nd:YAG laser frequency-doubled to 532 nm and using a spectral resolution of 5 cm^{-1}. The laser was operated with a power level of 45

* To whom correspondence should be addressed. E-mail: Iglesia@cchem.berkeley.edu; Bell@cchem.berkeley.edu.

10.1021/jp002419h CCC: $19.00
Published on Web 10/11/2000

mW, measured at the sample position with an optical power meter (Edmund Scientific). Samples (~50 mg) were pressed into a 9 mm diameter wafer at 350 MPa and placed within a Raman quartz flow cell. The wafers can be heated to 1073 K within the cell using a heating wire wound around the cell. The effect of laser heating was minimized by rotating the sample at 20 Hz. Raman spectra were recorded at 298 K after samples initially dried at 393 K were treated in 20% O_2/He (Scott Specialty Gases) at a given temperature for 1 h.

Mo K-edge X-ray absorption (XAS) spectra were measured using beamline 4-1 at the Stanford Synchrotron Radiation Laboratory (SSRL). The samples were diluted with boron nitride (BN) to about 5 wt % MoO_3, and they were then pressed into wafers, crushed, and sieved to retain particles with 0.18−0.25 mm diameter. These particles were placed within a thin quartz capillary tube (1.0 mm diameter; 0.1 mm wall thickness) and supported horizontally in the path of the rectangular X-ray beam (0.2 mm × 6.0 mm). The details of the in situ XAS cell used in XAS experiments were described elsewhere.[17] Transmission spectra were measured using Ar flow in three ion chamber detectors; one chamber was located before the sample to measure the incident X-ray intensity (I_0), one after the sample and before a Mo foil (7.5 μ) to measure the intensity after absorption (I_1), and one after the Mo foil in order to calibrate the energy scale (I_2). The sample spectra and the Mo foil reference spectra are reported as $\log(I_0/I_1)$ and $\log(I_1/I_2)$, respectively. The energy was calibrated using the first inflection point in the Mo foil spectrum (19.999 keV). Spectra were measured using a Si^{220} crystals monochromator with 5 eV energy increments in the pre-edge region (19.875−19.975 keV), 0.25 eV increments in the edge region (19.975−20.035 keV), and 0.04 $Å^{-1}$ in the fine structure region (20.035−21.024 keV). X-ray absorption data were analyzed using WinXAS software (version 1.2).[18,19] A linear fit to the pre-edge region was subtracted from the entire spectrum, and then the spectrum was normalized using a fifth-order polynomial fit to the post-edge fine structure (EXAFS) region.

Powder X-ray diffraction (XRD) patterns were measured at ambient conditions using a Siemens D-5000 diffractometer and Cu (Kα) radiation. A small amount of sample was distributed on a glass plate holder using a thin layer of Vaseline.

Results and Discussion

MoO_x Surface Density. The Mo surface densities per unit surface area were calculated from the MoO_3 concentration and the BET surface area measured using N_2 physisorption at 77 K; they are reported as the number of Mo atoms per nm^2 surface area (Mo/nm^2).[11] The Mo surface densities for MoO_x/ZrO_2 with varying Mo concentrations after treatment in dry air at 723, 773, or 873 K are shown in Figure 1. The polymolybdate saturation capacity on several metal oxide supports has been reported to be ~5 Mo/nm^2, from equilibrium adsorption measurement from aqueous molybdate solutions,[20−22] X-ray diffraction,[23−27] and X-ray photoelectron spectroscopy.[28,29] Those experimental results are in agreement with the theoretical monolayer coverage of 4.9 Mo/nm^2 calculated from the effective ionic diameter of MoO_6 octahedra.[30] It is apparent from Figure 1 that Mo surface densities for all MoO_x/ZrO_2 samples with Mo contents below 11 wt % MoO_3 are below this monolayer capacity

Bulk Structure of ZrO_2 and MoOx/ZrO_2 Samples Detected by X-ray Diffraction. The bulk structures of pure ZrO_2 and of supported MoO_x/ZrO_2 catalysts were determined by powder X-ray diffraction. X-ray diffraction patterns are shown

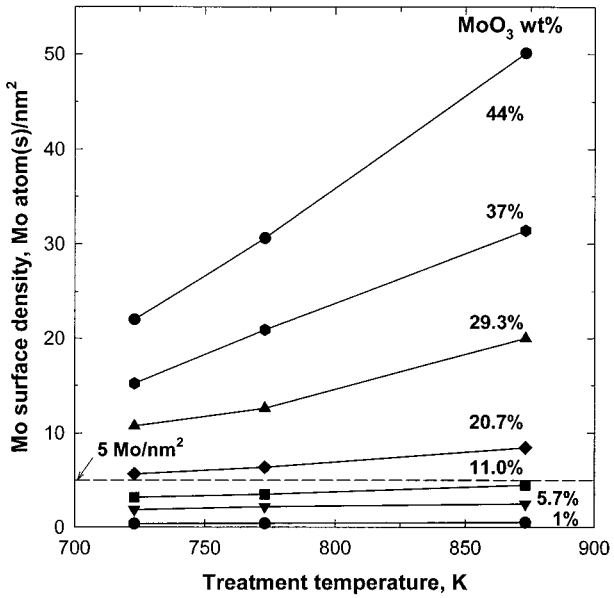

Figure 1. Mo surface densities of MoO_x/ZrO_2 catalysts with different MoO_3 loadings after treatment in dry air at 723, 773, and 873 K. The dashed line represents the MoO_x surface density corresponding to monolayer coverage, 5 Mo/nm^2.

in Figures 2A for the ZrO_2 support treated in air at 723, 773, or 873 K. Both tetragonal and monoclinic ZrO_2 phases were detected in all pure ZrO_2 samples and the monoclinic fraction increased with increasing treatment temperature (Figure 2D). Raman spectroscopy showed that amorphous $ZrO_x(OH)_{4-2x}$ begins to crystallize into tetragonal ZrO_2 at 673 K in 20% O_2/He; the tetragonal ZrO_2 formed is stable in dry air at temperatures up to 873 K.[31] No monoclinic ZrO_2 was detected in Raman experiments after amorphous $ZrO_x(OH)_{4-2x}$ was treated within the Raman cell in flowing 20% O_2/He at 873 K for 2 h (spectra not shown). Tetragonal ZrO_2, however, transformed into the monoclinic phase rapidly at room temperature when exposed to moist ambient air or to a H_2O vapor.[31] Clearly, X-ray diffraction detects monoclinic ZrO_2 because some tetragonal ZrO_2 converted to monoclinic when samples were exposed to moist ambient air during sample preparation and XRD measurements.

The incorporation of cations such as Mg^{2+}, Ca^{2+}, Y^{3+}, La^{3+}, Ce^{4+}, W^{6+}, and V^{5+}, into ZrO_2 inhibits the crystallization of amorphous $ZrO_x(OH)_{4-2x}$ into tetragonal ZrO_2 and the conversion of tetragonal ZrO_2 to the monoclinic phase.[10,32,33] The X-ray diffraction patterns for 1 wt % MoO_x/ZrO_2 suggest that tetragonal ZrO_2 is the predominant ZrO_2 phase; the volume fraction of monoclinic phase is 0.2, 0.31, and 0.4 for samples treated at 723, 773, and 873 K, respectively (Figure 2D). As the MoO_3 content increased to 11 wt %, only tetragonal ZrO_2 was detected in samples treated at 723−973 K (Figure 2B). At higher MoO_3 contents (37 wt %), both crystalline MoO_3 and $Zr(MoO_4)_2$ structures were detected along with some tetragonal ZrO_2 in samples treated at 723 or 773 K. The relative intensity of the $Zr(MoO_4)_2$ peaks increased with increasing treatment temperature (Figure 2C). Only crystalline $Zr(MoO_4)_2$ was detected after a 37 wt % MoO_3/ZrO_2 sample was treated at 873 K for 3 h (surface density 32 Mo/nm^2), suggesting that all MoO_3 reacts with ZrO_2 to form crystalline $Zr(MoO_4)_2$ at this temperature.

Solid-State Reactions of Crystalline MoO_3 with ZrO_2. The formation of $Zr(MoO_4)_2$ via solid-state reactions of MoO_3 and ZrO_2 was studied using an intimate physical mixture of

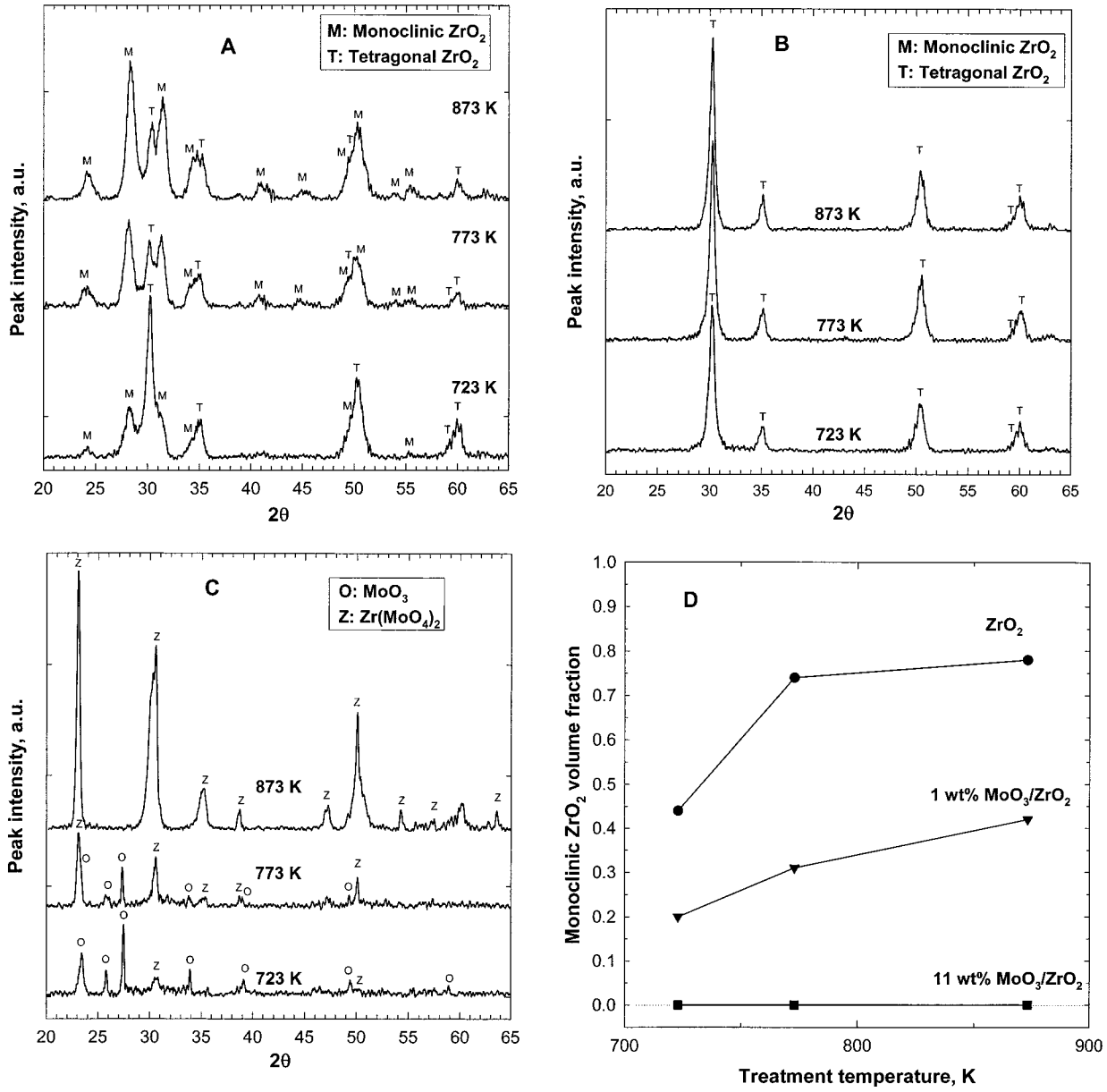

Figure 2. X-ray diffraction patters for pure ZrO_2 and MoO_x/ZrO_2 samples calcined in dry air at 723, 773, and 873 K: (A) pure ZrO_2; (B) 11 wt % MoO_x/ZrO_2; (C) 37 wt % MoO_x/ZrO_2. (D) Monoclinic ZrO_2 fraction in total ZrO_2 as functions of MoO_3 loading and treatment temperature.

crystalline MoO_3 and $ZrO_x(OH)_{4-2x}$ with the expected stoichiometry of $Zr(MoO_4)_2$ (Mo/Zr = 2). This mixture was mixed thoroughly by grinding with a mortar and a pestle for ~0.3 h in order to ensure homogeneity. It was then heated in 20% O_2 at 10 K/min with isothermal holds at specific temperatures; the resulting structural evolution was followed by Raman spectroscopy. The spectrum of this mixture at 298 K is identical to that for pure crystalline MoO_3,[14] with characteristic Raman bands at 118, 131, 159, 201, 220, 248, 287, 340, 370, 382, 474, 668, 821, and 998 cm^{-1} (spectrum a in Figure 3A). No new bands appeared after treating this mixture at 673 K for 1 h in 20% O_2/He. The treatment at 773 K for 1 h led to the appearance of two weak bands at ~741 and 943 cm^{-1} (spectra not shown), which suggest the formation of a new structure, apparently $Zr(MoO_4)_2$. The growth of these bands is very slow at 773 K and even at 873 K, but these bands became significantly more intense after heating at 973 K. At 973 K, the Raman bands at 141, 195, 232, 279, 373, 466, 660, and 820 cm^{-1}, corresponding to crystalline MoO_3, weakened with time and ultimately disappeared after ~0.25 h (Figure 3B). Concurrently, Raman bands at 736 and 939 cm^{-1}, corresponding to the new Mo compound, became more intense and then remained unchanged after the initial 0.25 h. After ~0.7 h at 973 K, the band at 334 cm^{-1} shifted to 333 cm^{-1} and the band at 990 cm^{-1} decreased in intensity during the first 0.25 h and then shifted to 983 cm^{-1} at longer times. The spectrum recorded at 298 K for this MoO_3-ZrO_2 mixture after treatment at 973 K is shown in Figure 3A (spectra b). It shows strong Raman bands at 177, 328, 361, 750, 945, and 1003 cm^{-1}. The absence of characteristic bands for crystalline MoO_3 or ZrO_2 suggests that the solid-state reaction is complete. The frequencies of Raman bands for MoO_3 and $Zr(MoO_4)_2$ in the spectra measured at 973 K (Figure 3B) are lower than those found in spectra measured at 298 K (Figure 3B), reflecting the contraction of MoO_3 and $Zr(MoO_4)_2$ crystalline lattice with decreasing temperature.[34]

The stable structure of $Zr(MoO_4)_2$ at 973 K is hexagonal with two-dimensional networks of MoO_4 tetrahedra and ZrO_6 octahedra (as illustrated in Figure 4).[35] The distance between two layers is 5.85 Å and neighboring layers interact via van der Waals forces between O atoms in different layers. The Mo^{6+}

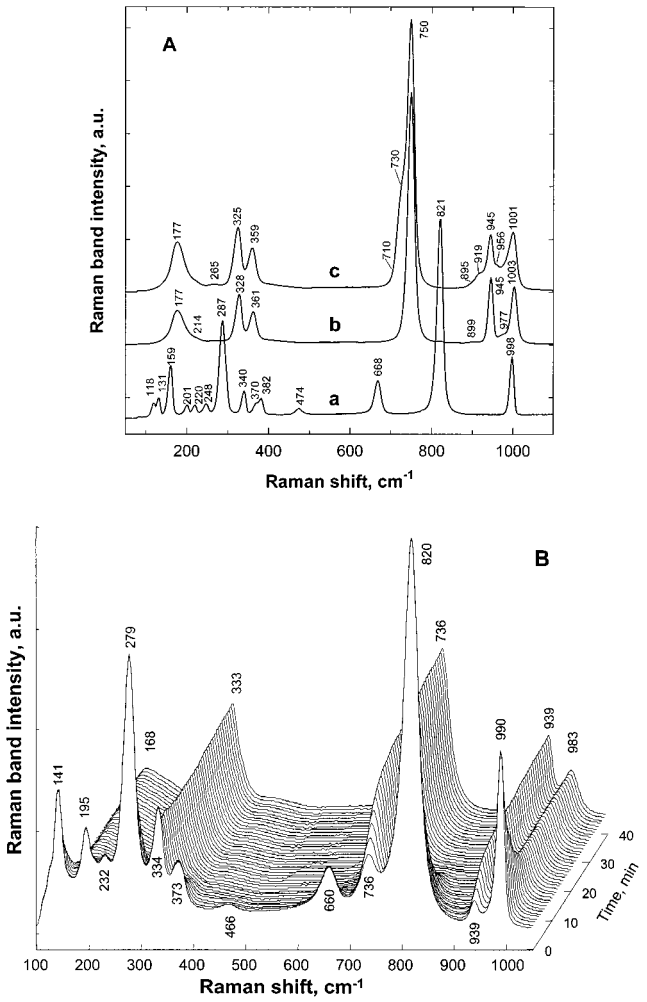

Figure 3. Raman spectra recorded for a physical mixture of MoO_3 and $ZrO_x(OH)_{4-2x}$ (Mo/Zr atomic ratio = 2:1). (A) a, before treatment at high temperatures; b, after treatment at 973 K in 20% O_2/He for 40 min; c, after evacuated at 973 K for 2 min and then equilibrated in 69 kPa $^{18}O_2$ at 1023 K for 15 min. All spectra were recorded at 298 K. (B) Spectra recorded during treatment in 20% O_2 at 973 K with intervals of 1 min.

cations are present in distorted tetrahedral coordination, with one O atom bonded only to Mo and the other three O atoms shared by Mo and Zr atoms. This structure gives rise to two types of Mo—O distances: a shorter bond at 1.690 Å and three longer bonds at 1.763, 1.762, and 1.767 Å, respectively. The resulting tetrahedral O═MoO_3 species in $Zr(MoO_4)_2$ have approximate C_{3v} symmetry.

For a tetrahedral MX_4 species of T_d symmetry, all four normal modes of vibration are Raman-active and the ν_2(E) and $\nu_4(F_2)$ modes are often too similar in frequency to be detected as separate bands.[36,37] For tetrahedral MoO_4^{2-}(aq), these four vibration modes, $\nu_1(A_1)$, $\nu_3(F_2)$, and ν_2 (ν_4) are found at 897, 837, and 317 (317) cm^{-1}, respectively.[38] When the symmetry of MX_4 species decreases from T_d to C_{3v}, as in the case of O═MoO_3 in $Zr(MoO_4)_2$, both $\nu_3(F_2)$ and $\nu_4(F_2)$ split into two modes (A_1 + E).[36] We assign the 1003 cm^{-1} band for $Zr(MoO_4)_2$ to the vibration of the shorter Mo—O bonds and the bands at 945 and 750 cm^{-1} to antisymmetric and symmetric ν(O—Mo—O) stretchings of the longer Mo—O bonds. The bands at 328 and 361 cm^{-1} are assigned to the δ(Mo—O) deformation modes and the band at 214 cm^{-1} to the ρ_r(Mo—O) rocking mode. The band at 177 cm^{-1} appears to arise from lattice vibration modes.

These band assignments were confirmed by ^{18}O exchange studies, in which some of the lattice ^{16}O atoms in $Zr(MoO_4)_2$ were replaced with ^{18}O. The Raman spectrum (spectra c in Figure 3A) for partially ^{18}O-exchanged $Zr(MoO_4)_2$ showed new bands at 710 (weak), 730, 895 (weak), 919, and 956 cm^{-1}. The estimated frequencies for Mo—^{18}O stretching and ^{16}O—Mo—^{18}O symmetric and antisymmetric vibration are 954, 920, and 730 cm^{-1}, respectively. These values were calculated by assuming that the force constants for Mo—O bonds do not change upon ^{18}O isotopic substitution and that the vibration frequencies are inversely proportional to the square root of the reduced mass in the assumed harmonic oscillator.[37] These estimates agree with the observed frequencies. Unresolved broader bands were also detected at ~710 and ~895 cm^{-1}, but their frequencies cannot be determined accurately because they overlap with stronger bands. Spectra b and c in Figure 3A show that the intensity ratio of the antisymmetric ν(O—Mo—O) band (945 cm^{-1}) to the ν(Mo═O) band (1003 cm^{-1}) decreased from 1.15 to 0.96 after ^{18}O isotopic substitution, suggesting that

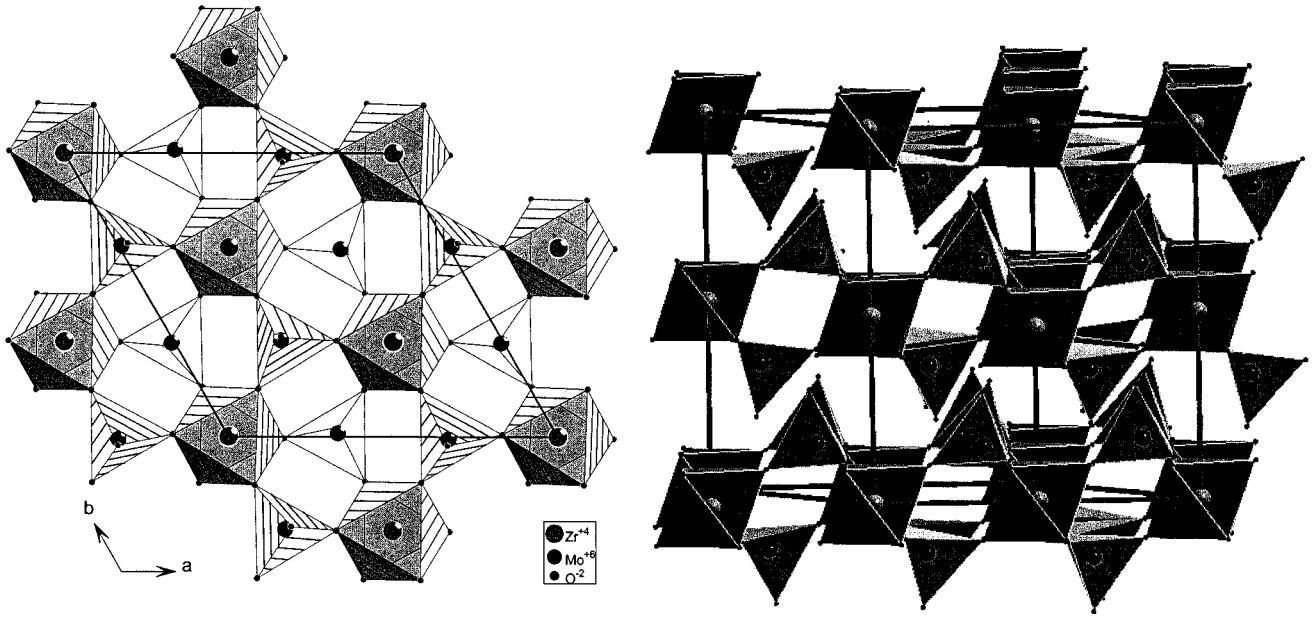

Figure 4. Crystal structure of hexagonal $Zr(MoO_4)_2$. The figures were drawn using structural parameters from ref 33.

bridging O atoms exchange with gas phase $^{18}O_2$ more rapidly than O atoms in terminal Mo═O groups.

Solid-state reactions of crystalline MoO_3 with ZrO_2 were also studied by X-ray absorption spectroscopy. X-ray absorption spectra can be divided into two parts, defined in terms of the energy range and the information provided by each region. The absorption edge position and the spectral features near the edge (XANES) reflect the oxidation state and coordination symmetry of the absorber. The extended X-ray absorption fine structure (EXAFS) arises from scattering of the ejected photoelectrons by neighboring atoms and it reflects the local structure around the absorber.[16] For molybdenum oxides, the Mo−K edge detected at ∼20 keV corresponds to the ejection of an Mo 1s electron, while the pre-edge feature at ∼19.99 keV arises from 1s to 4d electronic transitions that are dipole-forbidden in centrosymmetric structures.[39] The Mo^{6+} cations in MoO_3 adopt off-center positions within distorted MoO_6 octahedra and this distortion allows these forbidden transitions to occur. The intensity of this pre-edge feature increases as the Mo^{6+} centers acquire tetrahedral symmetry, as a result of greater p−d orbital mixing in Mo^{6+} tetrahedra.[40]

The Mo−K near-edge spectra (Figure 5A) and the radial structure functions obtained from the fine structure region (Figure 5B) for a mixture of MoO_3 and $ZrO_x(OH)_{4-2x}$ after treatment at various temperatures are shown in Figure 5. Both the near-edge spectrum and the radial structure functions of the $MoO_3/ZrO_x(OH)_{4-2x}$ physical mixture are initially similar to bulk MoO_3. After this mixture was treated at 723 K for 3 h, the near-edge spectrum changed significantly, but without an observable change in the intensity of the pre-edge feature. The radial structure functions remain unchanged, but the intensity of the peak corresponding to Mo−Mo neighbors (maximum at 3.17 Å) decreased (Figure 5B). These results suggest that thermal treatment at 723 K led to the dispersion of bulk MoO_3 onto the ZrO_2 surface with a consequent decrease in MoO_3 domain size, but without any reaction between MoO_3 and ZrO_2, which would have changed the local coordination. At 973 K, the pre-edge feature became stronger and the scattering peak corresponding to the Mo−Zr next nearest neighbor shell in the radial structure function also increased in intensity (curve d in Figure 5A,B), reflecting the formation of bulk $Zr(MoO_4)_2$. The scattering peak due to the Mo−Mo shell in the radial structure functions disappeared and a new feature, corresponding to a Mo−Zr shell (with a maximum at 3.45 Å), became clearly visible (Figure 5B). The more intense pre-edge peak for $Zr(MoO_4)_2$ relative to that of MoO_3 is consistent with the tetrahedral environment of Mo^{6+} ions in $Zr(MoO_4)_2$. For the sample treated at 873 K for 3 h, both the near-edge spectrum and the radial structure function (curve c in Figure 5A,B) are similar to those obtained for $Zr(MoO_4)_2$. The pre-edge peak is more intense than that for the sample treated at 723 K but is less intense than that for $Zr(MoO_4)_2$. The radial structure function shows a scattering peak with a maximum at 3.37 Å (curve c in Figure 5B), which lies between 3.17 and 3.45 Å and which may reflect overlapping Mo−Mo and Mo−Zr scattering features. These results for the sample treated at 873 K show that the reaction of MoO_3 and ZrO_2 starts at ∼873 K.

Effect of Treatment Temperature and Mo Content on MoO_x/ZrO_2 Structure. The Raman spectra of supported molybdenum oxides and their structural interpretation have recently been reviewed by Mestl and Srinivasan.[14] Supported molybdenum oxides can exist as MoO_x monomers, two-dimensional polymolybdates, and bulk MoO_3. The dependence of the structure of dispersed MoO_x on Mo concentration, pH of impregnation solution, thermal treatment temperature, and oxide support were previously examined.[14,41−45] These studies have concluded that the structure of supported MoO_x species depends strongly on the identity of the oxide support, on the Mo content, and on the treatment temperature, but only weakly on the solution pH and on the type of soluble Mo precursor used. Since hydration of supported MoO_x samples by exposure to ambient moisture can alter their Raman spectra,[45−49] all spectra in our study were obtained after in situ treatment at the specified temperatures within the Raman cell.

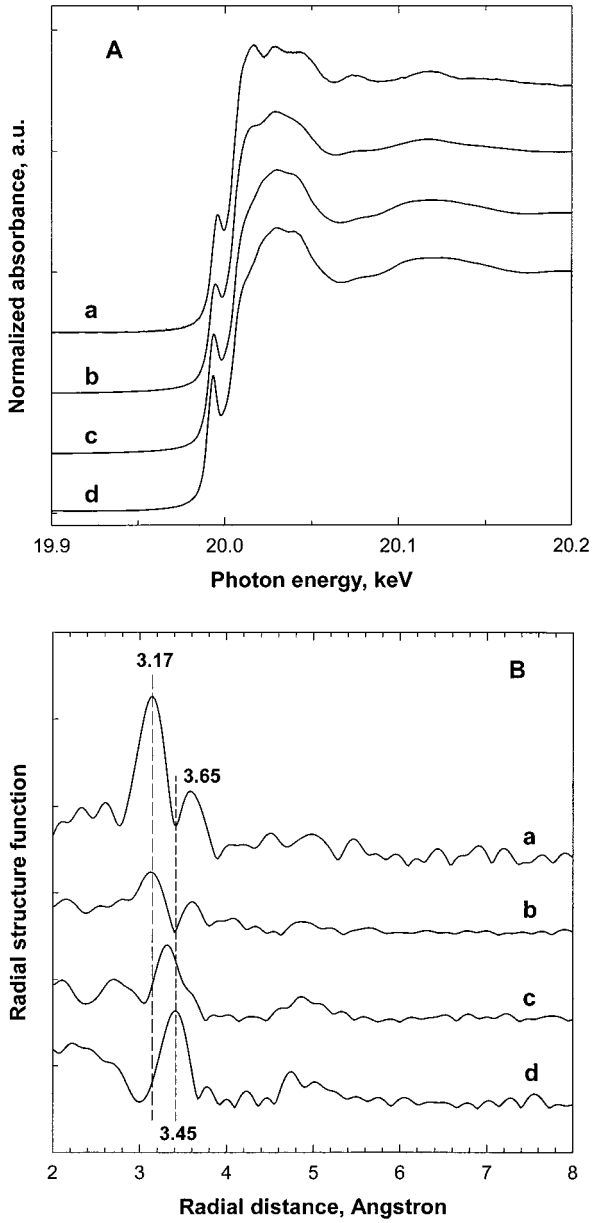

Figure 5. Near-edge X-ray absorption spectra (A) and radial structure function (B) of a physical mixture of MoO_3 and $ZrO_x(OH)_{4-2x}$ (Mo/Zr atomic ratio = 2:1) after treatment in 20% O_2/He at different temperatures: (a) ambient; (b) 723 K for 3 h; (c) 873 K for 3 h; (d) 973 K for 3 h.

The Raman spectra for 1 wt % MoO_3/ZrO_2 samples treated in 20% O_2/He for 1 h at various temperatures are shown in Figure 6. Spectrum a shows broad bands at 168, 402, 523, 859, 940, 970, and 1086 cm^{-1} after treatment at 393 K. The band at 1086 cm^{-1} arises from carbonate species formed on ZrO_2 by reaction with ambient CO_2. The Raman bands at 168, 402, and

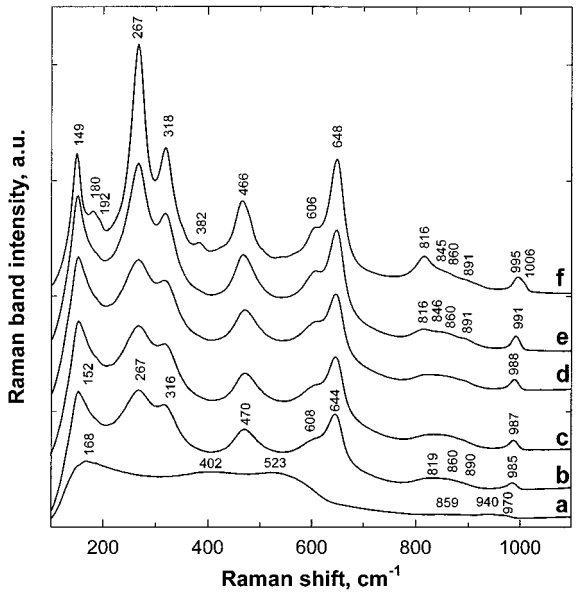

Figure 6. Raman spectra recorded at 298 K for 1 wt % MoO_x/ZrO_2 sample after pretreatment in 20% O_2/He for 1 h at different temperatures: (a) 393 K; (b) 673 K; (c) 723 K; (d) 773 K; (e) 873 K; (f) 973 K.

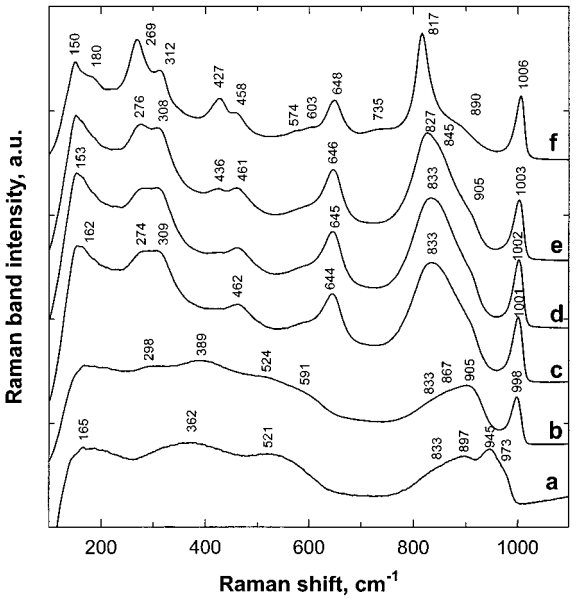

Figure 7. Raman spectra recorded at 298 K for 11 wt % MoO_x/ZrO_2 sample after pretreatment in 20% O_2/He for 1 h at different temperatures: (a) 393 K; (b) 673 K; (c) 723 K; (d) 773 K; (e) 873 K; (f) 973 K.

523 cm^{-1} are assigned to amorphous $ZrO_x(OH)_{4-2x}$. The bands at 940 and 970 cm^{-1} arise from Mo═O stretching modes of dispersed polymolybdates and the broad band centered at 859 cm^{-1} is assigned to monomeric MoO_4 species.[14]

Treatment at 673 K led to the appearance of a distinct band at ~985 cm^{-1} along with overlapping broad bands in the 800−900 cm^{-1} region. The band at ~985 cm^{-1} is assigned to the Mo═O stretching mode in MoO_6 octahedra within two-dimensional polymolybdates. This band shifts to higher frequencies with increasing treatment temperature, apparently as a result of MoO_x domain growth. An increase in Mo═O frequencies with increasing polymolybdate cluster size has been reported previously.[48−50] This finding is consistent with UV−visible data, which showed the absorption energy of the 1 wt % MoO_x/ZrO_2 sample decreased with increasing pretreatment temperature.[11] The decreasing UV−vis absorption edge energy indicates that MoO_x domains grow with increasing pretreatment temperature.[51] The observed ν(Mo═O) stretches at wavenumbers above 980 cm^{-1} suggests that two-dimensional polymolybdate species exist even in 1 wt % MoO_3 samples, despite their low Mo surface density (<1 Mo/nm^2). Recently, Xiong et al.[52] reported that octahedral polymolybdate species were detected by UV resonance Raman spectroscopy even at very low Mo contents (0.1 wt %) on α-Al_2O_3. The broad bands at 800−900 cm^{-1} become more clearly resolved after treatment at 873 or 973 K, probably because the structure of MoO_x monomers becomes more uniform after annealing at high temperature.

At least four distinct Raman bands were detected in the 800−900 cm^{-1} range (at 816, 845, 860, and 891 cm^{-1}, respectively) for the sample treated at 873 K. After treatment at 973 K, the band at 816 cm^{-1} became sharper and a band at 1006 cm^{-1} appeared as a shoulder in the Mo═O band at 995 cm^{-1}. The bands at 816 and 1006 cm^{-1} were assigned to antisymmetric ν(O−Mo−O) and ν(Mo═O) in a MoO_5 tetragonal−pyramidal structure, O═Mo(O−Zr)$_4$. The ν(Mo═O) modes in tetragonal−pyramidal $[O{=}MoCl_4]^-$,[53] O═MoF_4,[54,55] and O═$MoCl_4$[56,57] were observed at 1008, 1015, and 1048 cm^{-1}, respectively. Desikan et al.[58] assigned the Raman band observed on 12 wt % MoO_3/Al_2O_3 at 1010 cm^{-1} to ν(Mo═O) of a monooxo O═Mo(O−Al)$_4$ species, the structure of which was proposed earlier by Payen et al.[48] and Stencel et al.[49] The bands at 891 and 845 cm^{-1} were assigned to the antisymmetric and symmetric ν(O═Mo═O) modes in isolated MoO_4 tetrahedra, by analogy with the assignments of bands at 897 and 827 cm^{-1} to these modes in aqueous MoO_4^{2-} ions.[38] The band at 860 cm^{-1} may arise from a less distorted MoO_4 species than those for the 891 cm^{-1} band. The structure of the ZrO_2 support in the 1 wt % MoO_3/ZrO_2 sample also changed with increasing temperature and tetragonal ZrO_2 was detected after treatment at 673 K for 1 h by its Raman bands at 152, 267, 316, 470, 608, and 644 cm^{-1}.[59] Tetragonal ZrO_2 was stable up to 873 K. Monoclinic ZrO_2 bands at 180, 192, and 382 cm^{-1} appeared after treatment at 973 K and higher temperatures.[60]

Mo surface densities approach polymolybdate monolayer values (~5 Mo/nm^2) for 11 wt % MoO_x/ZrO_2 samples after treatment at temperatures above 723 K (Figure 1). After treatment at 393 K, the Raman spectra for this sample showed bands at 973, 945, 897, 833 (sh), 521, and 362 cm^{-1} (Figure 7). The bands at 945 and 973 cm^{-1} were assigned to ν(Mo═O) modes in MoO_6 octahedra within polymolybdate domains.[14] More specifically, the band at 945 cm^{-1} may arise from $Mo_5O_{16}^{2-}$ species (see discussion below). Treatment in air at 673 K caused the Raman bands at 945 and 973 cm^{-1} to coalesce into one band at 998 cm^{-1}, and the band at 897 cm^{-1} to shift to 905 cm^{-1}. The shift of the bands at 945 and 973 cm^{-1} to higher frequencies reflects the dehydration of the sample at 673 K; physisorbed H_2O weakens Mo═O bonds and it causes the ν(Mo═O) in MoO_x species to shift to lower frequencies.[45−49] The shift of the 897 cm^{-1} band to 905 cm^{-1} for isolated tetrahedral MoO_4 species on Al_2O_3 was attributed by Jeziorowski et al.[42] and Wang et al.[44] to interactions with the Al_2O_3. Treatment at 723 K caused the 905 cm^{-1} band to weaken gradually and the 833 cm^{-1} band to become more intense until it emerged as the most intense band in the 800−900 cm^{-1} region (Figure 8B,C). The ν(Mo═O) frequency shifted from 998 to 1001 cm^{-1} and became stronger after samples were treated in air at 723 K. The more intense bands for symmetric ν(Mo−O−Mo) (833 cm^{-1}) and ν(Mo═O) (998−1001 cm^{-1}) modes in octahedral polymolybdates became stronger at the expense of the bands for isolated MoO_4 tetrahedra [ν(O═Mo═O) at

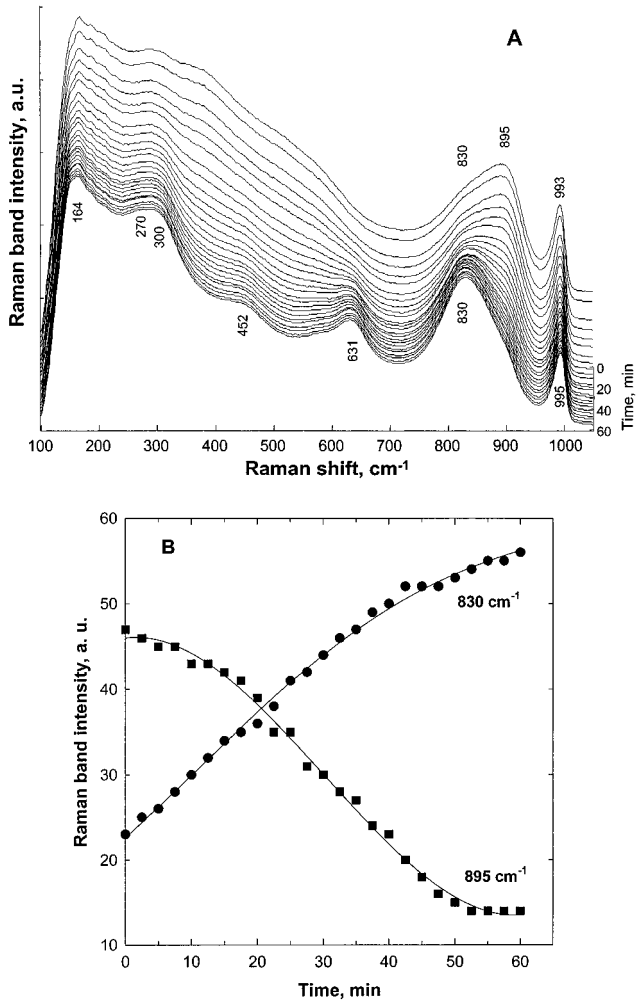

Figure 8. Raman spectra recorded at 723 K in 20% O_2/He for 11 wt % MoO_x/ZrO_2 sample after temperature was increased from 673 K (A) and intensities of Raman bands at 830 and 895 cm^{-1} as a function of time (B). The time axis represents the time length for the sample to stay at 723 K after the temperature was increased rapidly from 673 K.

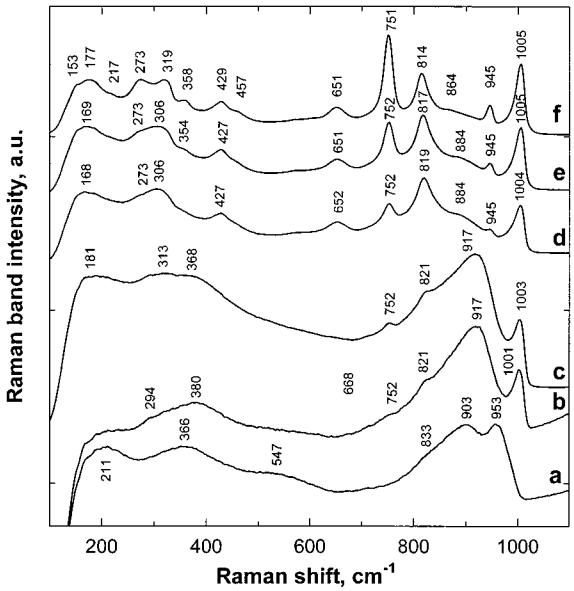

Figure 9. Raman spectra recorded at 298 K for 20.7 wt % MoO_x/ZrO_2 sample after pretreatment in 20% O_2 for 1 h at different temperatures: (a) 393 K; (b) 723 K; (c) 773 K; (d) 823 K; (e) 873 K; (f) 973 K.

$\sim$905 cm^{-1}]. These data suggest that isolated MoO_4 tetrahedra condense to form octahedral polymolybdate domains by forming bridged Mo—O—Mo bonds as the surface area of the ZrO_2 support decreases with increasing treatment temperature.

The Raman spectra for 11 wt % MoO_x/ZrO_2 samples treated at 773 and 873 K resemble those for samples treated at 723 K (Figure 7), but the frequency of the Mo═O stretching band at 1001 cm^{-1} was slightly shifted to 1002 and 1003 cm^{-1}. An intense band appeared at 817 cm^{-1} after treatment of 973 K along with a new band at 1006 cm^{-1}. These two new bands reflect the formation of tetragonal−pyramidal O═MoO_4 species (see discussion above). The weakening of the 833 cm^{-1} band after treatment at 973 K suggests the formation of tetragonal−pyramidal O═MoO_4 species via dissociation of Mo—O—Mo bonds in polymolybdate species.

For samples with low Mo concentrations (11 wt %), neither Raman spectroscopy nor X-ray diffraction detected bulk MoO_3 or $Zr(MoO_4)_2$ structures because the MoO_x surface density of these samples remained well below the monolayer value of $\sim$5 Mo/nm^2 at all treatment temperatures. Bulk MoO_3 is expected to form in samples with higher MoO_x surface densities; this was detected by Raman in the 20.7 wt % MoO_x/ZrO_2 sample (Figure 9). The Raman bands detected at 752 and 821 cm^{-1} after treatment at 723 or 773 K arise from crystalline $Zr(MoO_4)_2$ and MoO_3, respectively. The band at 917 cm^{-1} appears to correspond to the symmetric ν(O═Mo═O) modes in highly distorted MoO_4 tetrahedra;[42] it disappeared after treatment at temperatures above $\sim$823 K, suggesting that tetrahedral MoO_4 species oligomerize upon heating. The ν(Mo═O) bands appeared above 1000 cm^{-1} and they shifted to higher wavenumbers with increasing treatment temperature. A new band at $\sim$651 cm^{-1} emerged in samples treated above 823 K; it can be assigned to the symmetric ν(Mo—O—Zr) mode in O═MO_4 tetragonal−pyramidal structures, by analogy with the assignment of 668 cm^{-1} to symmetric Mo—O—Mo stretching in MoO_3. The bands at 752 and 945 cm^{-1} became more intense with increasing treatment temperature, as expected from the gradual formation of crystalline $Zr(MoO_4)_2$ as the treatment temperature increased.

Raman spectra for the 37 wt % MoO_x/ZrO_2 sample are shown in Figure 10. After treatment at 393 K, Raman bands were detected at 211, 343, 378 (sh), 447 (w), 601 (w), 663 (w), 692 (w), 756 (w), 842, 885, 927 (sh), 950, and 970(sh) cm^{-1}. This spectrum resembles that for ammonium pentamolybdate (spectrum a in Figure 10; $(NH_4)_4Mo_5O_{17}\cdot 2H_2O$), which is a product of AHM decomposition at 373 K.[61,62] The structure and chemical composition of this pentamolybdate species derived from AHM thermal decomposition was verified using X-ray diffraction and thermogravimetry.[62] MoO_x species exist predominantly as two-dimensional oligomeric domains after treatment at 393 K. Crystalline MoO_3 Raman bands appear at 200, 219, 246, 288, 339, 379, 668, 821, and 998 cm^{-1} (Figure 9) after treatment at 723 or 773 K. The presence of bands at $\sim$750 and 945 cm^{-1} shows that bulk $Zr(MoO_4)_2$ coexists as a minority species with bulk MoO_3 in these samples. $Zr(MoO_4)_2$ bands become more intense with increasing treatment temperature at the expense of weaker MoO_3 bands, suggesting that $Zr(MoO_4)_2$ forms via reaction of MoO_3 crystallites with ZrO_2, as discussed earlier. Zirconium molybdate became the predominant species after treatment at 873 or 973 K; its characteristic Raman bands at 177, 328, 360, 750, 945, and 1004 cm^{-1} increased in intensity and the bands for bulk MoO_3 disappeared in the spectrum for the sample treated at 973 K. The weak bands at 651 and 814 cm^{-1} remained even after treatment at 973 K, suggesting the residual presence of O═MO_4 tetragonal−pyramidal species. The

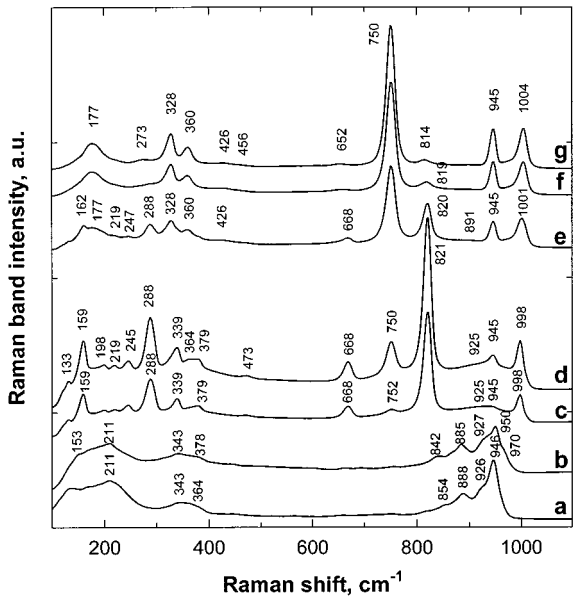

Figure 10. Raman spectra recorded at 298 K for 37 wt % MoO_x/ZrO_2 sample after pretreatment in 20% O_2 for 1 h at different temperatures: (b) 393 K; (c) 723 K; (d) 773 K; (e) 823 K; (f) 873 K; (g) 973 K. (a) Spectrum of $Mo_5O_{17}^{4-}$, which was formed by decomposing $(NH_4)_7Mo_7O_{24}{\cdot}4H_2O$ at 373 K for 1 h.

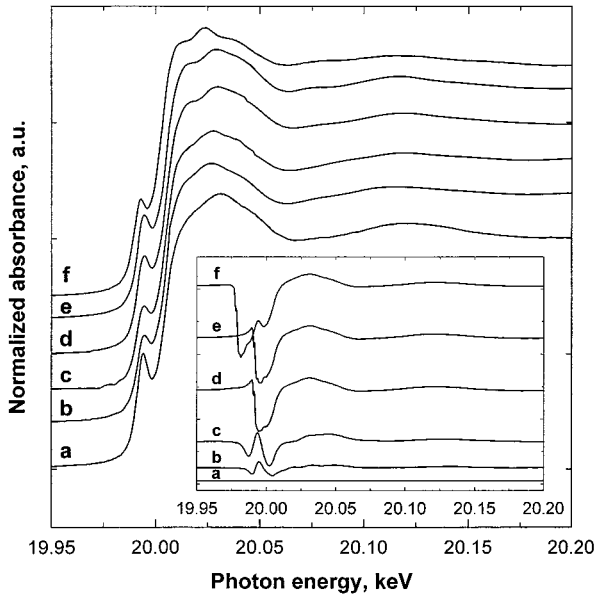

Figure 11. Near-edge X-ray absorption spectra of MoO_x/ZrO_2 samples and standard compounds: (a) ammonium bimolybdate ($(NH_4)_2Mo_2O_7$); (b) 5.7 wt % MoO_x/ZrO_2; (c) 11 wt % MoO_x/ZrO_2; (d) 37 wt % MoO_x/ZrO_2; (e) 44 wt % MoO_x/ZrO_2; (f) ammonium heptamolybdate ($(NH_4)_7Mo_7O_{24}{\cdot}4H_2O$). The inset shows the difference spectra for each sample relative to the ammonium bimolybdate spectrum.

Raman spectra obtained for 29.7 and 44 wt % MoO_x/ZrO_2 at a given treatment temperature and the conclusions reached from them are essentially the same as those for the 37 wt % MoO_x/ZrO_2 samples; therefore, their Raman spectra are not shown.

Changes in MoO_x structure with changes in MoO_3 concentration and treatment temperature were also studied using X-ray absorption spectroscopy. Figure 11 shows the near-edge spectra of MoO_x/ZrO_2 with different MoO_3 concentrations treated at 723 K and also the spectra for two model compounds [ammonium bimolybdate (ABM) and ammonium heptamolybdate (AHM)]. The difference spectra for each sample relative to the ABM spectrum are shown in the inset of Figure 11. Near-edge

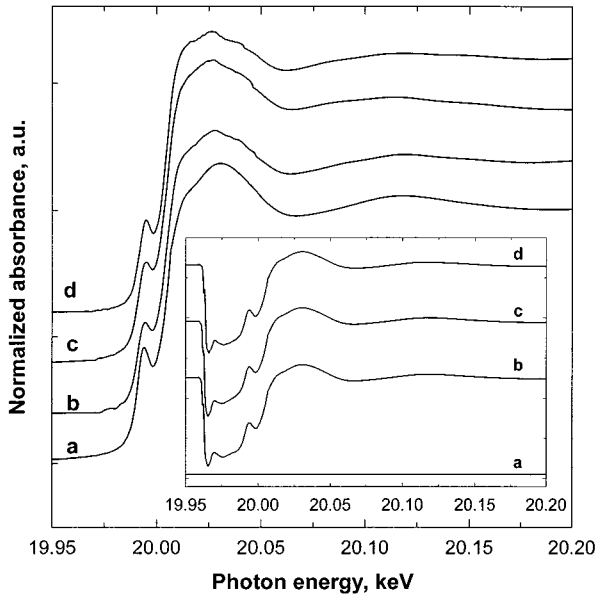

Figure 12. Near-edge X-ray absorption spectra of 11 wt % MoO_x/ZrO_2 samples treated at different temperatures: (a) 393 K; (b) 723 K; (c) 873 K; (d) 973 K. The inset shows the difference spectra for each sample relative to the spectrum of the 393 K treated sample.

X-ray absorption spectra can be used to probe changes in local structure and electronic properties by comparing them with the near edge features in relevant reference compounds.[63−65] For MoO_x/ZrO_2 samples with Mo surface densities below monolayer coverage (~5 Mo/nm^2), the near-edge spectra (curves b and c in Figure 11) resemble more closely the spectrum of ABM than that of AHM (insert in Figure 11). As the MoO_3 concentration increased from 11 wt % to 37 and 44 wt %, the near-edge spectra (curves d and e in Figure 11) gradually became similar to that for AHM (curve f), suggesting that MoO_x domains increase in size as the MoO_3 concentration increases.

The near-edge spectra of 11 wt % MoO_x/ZrO_2 samples treated at several temperatures (393, 723, 873, and 973 K) are shown in Figure 12, and the difference spectra for each sample relative to that for the sample treated at 393 K are also shown in the inset of Figure 12. The spectrum for the sample treated at 393 K shows a more intense pre-edge feature than the other samples, reflecting a higher fraction of tetrahedral Mo^{6+} species than in the samples treated at higher temperatures. This observation is consistent with the Raman spectra shown in Figure 7 (spectrum a vs spectra c, e, and f). The pre-edge feature becomes slightly more intense with increasing treatment temperature for samples treated at 723, 873, and 973 K; this reflects the conversion of MoO_x octahedral species to less symmetrical tetragonal−pyramidal MoO_x structures.

In summary, isolated tetrahedral MoO_4, two-dimensional polymolybdates, tetragonal−pyramidal O═MoO_4, crystalline MoO_3, and $Zr(MoO_4)_2$ were detected by Raman spectroscopy in MoO_x/ZrO_2 samples with 1−44 wt % MoO_3 (0.35−50 Mo/nm^2) after treatment in 20% O_2/He at 393−973 K. MoO_x species present on ZrO_2 at low and high Mo surface densities differ markedly; a distinct transition between molybdate oligomers and bulk MoO_3 crystallites occurs at Mo surface densities of ~5 Mo/nm^2. At lower surface densities (<5 Mo/nm^2), only two-dimensional MoO_x oligomers are detected by Raman spectroscopy, without any evidence for bands corresponding to three-dimensional MoO_3 clusters (821 cm^{-1}) or $Zr(MoO_4)_2$ (751 cm^{-1}). Raman bands at 751 and 821 cm^{-1} were only observed as MoO_3 crystallites at Mo surface densities of 5 Mo/nm^2 or

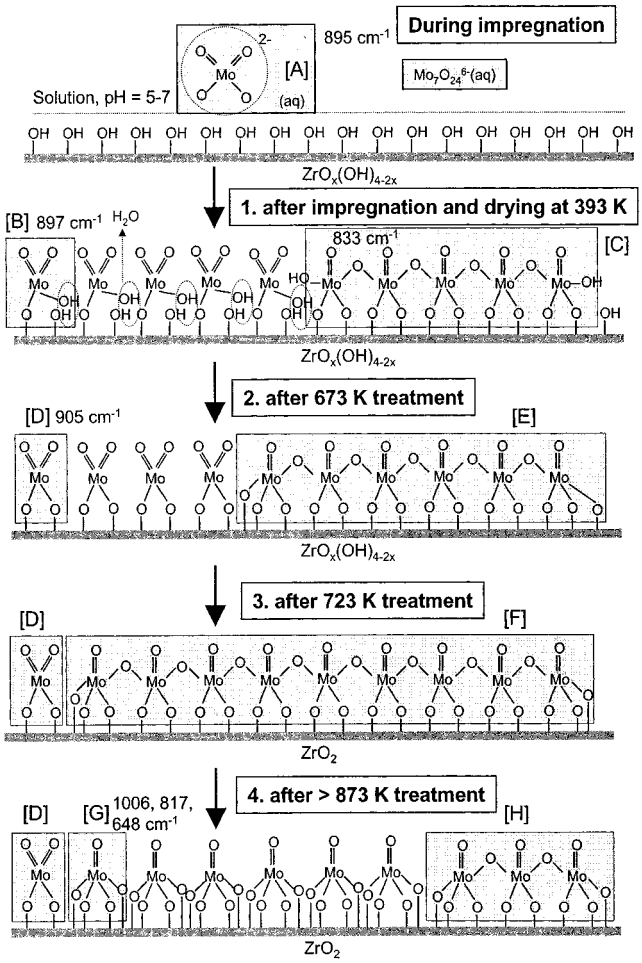

Figure 13. MoO_x structure evolution of MoO_x/ZrO_2 samples with Mo surface density <5 Mo/nm^2.

higher; they react with ZrO_2 at temperatures above 873 K but remain as MoO_3 crystallites at lower temperatures.

The treatment temperature also plays an important role in determining the structure of MoO_x/ZrO_2 catalysts. Two samples, 11 and 37 wt % MoO_3/ZrO_2, for which Mo surface densities are below and above the monolayer coverage, respectively, are used to illustrate the structure evolution as the conditions of the thermal treatment are changed (Figure 13). The Raman spectrum for aqueous AHM solution at a pH of 6 showed that both isolated MoO_4^{2-} (species [A] in Figure 13) and $Mo_7O_{24}^{6-}$ ions coexist in solution, and they show their characteristic bands at 895 and 934 cm^{-1}, respectively (spectra not shown). These two types of MoO_x species were preserved after the initial impregnation of $ZrO_x(OH)_{4-2x}$ with this solution and drying at room temperature. After drying at 393 K, the 11 wt % MoO_x/ZrO_2 sample contained only isolated MoO_4 tetrahedra (species [B] in Figure 13) and two-dimensional molybdate oligomers with five or more Mo atoms (species [C] in Figure 13), as shown by the presence of Raman bands at 897 cm^{-1} and at 945 and 973 cm^{-1} (spectrum a in Figure 7). After treatment at 673 K, species [B] were anchored to the ZrO_2 surface via two Mo—O—Zr linkages to form tetrahedral monomolybdate species ([D] in Figure 13), giving rise to the band at 905 cm^{-1} (spectrum b in Figure 7). Species [D] adopted a more distorted tetrahedral structure than species [B]; this distortion may be responsible for the observed shift of the 897 cm^{-1} band to 905 cm^{-1} after treatment air at 673 K (spectra a and b in Figure 7).[42] This treatment did not appear to increase the size of MoO_x domains, because the 833 cm^{-1} band for Mo—O—Mo did not change in intensity or frequency after treatment at 673 K (Figure 7). The bands at 945 and 973 cm^{-1} shifted to 998 cm^{-1} after treatment at 673 K, apparently as a result of dehydration. When the sample was cooled to 298 K after treatment at 673 K and then exposed to 3.0 kPa H_2O, the spectrum a in Figure 7 was restored. The presence of physically adsorbed or weakly chemisorbed H_2O or a higher concentrations of surface hydroxyl species may lead to weaker Mo═O bonds and to a shift in the Mo═O frequencies to lower wavenumbers.[45,48,49]

The amorphous zirconia support in the 11 wt % MoO_x sample also underwent structural changes upon treatment at high temperature; it crystallized into its tetragonal crystal structure at 723 K and the surface area concurrently decreased.[11] The presence of tetragonal ZrO_2 was confirmed by X-ray diffraction and Raman spectroscopy (Figure 2C and spectrum c in Figure 7). The distance among isolated surface MoO_x species decreases as the ZrO_2 surface area decreases and the isolated MoO_x must restructure to form MoO_x oligomers with Mo—O—Mo bonds. Oligomerization of MoO_x was first detected at 723 K in the 11 wt % MoO_x/ZrO_2 sample, suggested by the increase in the intensity of the Raman band for bridging Mo—O—Mo stretching at 833 cm^{-1} (Figure 8A,B). The concurrent decrease in the intensity of the 905 cm^{-1} band suggests that domain growth occurs at the expense of isolated MoO_4 tetrahedral species.

Oligomeric MoO_x species were stable at temperatures below 873 K in the 11 wt % MoO_x/ZrO_2 sample; the Raman spectra after treatment at 773 or 873 K resembled that obtained after treatment at 723 K. Significant structural changes occurred at 973 K, as illustrated in Figure 13 (step 4). Bridging Mo—O—Zr bonds (817 cm^{-1}) were formed at the expense of Mo—O—Mo bonds (833 cm^{-1}) in octahedral polymolybdates (spectra e and f in Figure 7). The resulting species [G] in Figure 13 can adopt a tetragonal—pyramidal structure, which gives arise to Raman bands at 817 and 1006 cm^{-1} (assigned to a Mo—O—Zr antisymmetric stretching mode and a ν(Mo═O) vibration mode, respectively). The antisymmetric nature of the 1006 cm^{-1} band suggests that an unresolved additional band may be present at its low wavenumber side; this unresolved band appears to reflect the ν(Mo═O) band in the remaining unreacted polymolybdates. These observations, and the broader band on the high wavenumber side of the sharper 817 cm^{-1} band, suggest that some polymolybdate domains remain even after treatment at 973 K. The Raman bands at 1001—1003 cm^{-1} detected after treatment at 723—873 K (Figure 7) may reflect overlapping ν(Mo═O) bands in polymolybdates (998 cm^{-1}) and in isolated tetragonal—pyramidal MoO_x species (1006 cm^{-1}). The shift of this composite band to higher frequencies with increasing treatment temperature may then reflect the increasing abundance of the tetragonal—pyramidal species [G].

MoO_x species formed at high temperatures (>673 K) differ markedly in samples with low and high surface density. The predominant MoO_x species in 37 wt % MoO_3/ZrO_2 after drying at 393 K resembles a pentamolybdate structure with Raman bands at 950, 927, and 885 cm^{-1} (Figure 10). The formation of pentamolybdate by decomposition of heptamolybdate at 393 K was confirmed by independent studies of the thermal decomposition of bulk ammonium heptamolybdate.[61,62] Both MoO_3 and $Zr(MoO_4)_2$ formed after treatment at 723 K, as shown by Raman and X-ray diffraction data. The presence of crystalline MoO_3 is evident from its strong Raman bands at 821 and 998 cm^{-1} and the presence of $Zr(MoO_4)_2$ form its Raman bands at 750 and 945 cm^{-1} (Figure 10). For samples treated below 873 K, MoO_3 was the most abundant species and $Zr(MoO_4)_2$ was a minor component. Crystalline MoO_3 was not detected in the

37 wt % MoO_x/ZrO_2 sample after treatment at 873 K for 1 h and the predominant bulk $Zr(MoO_4)_2$ species coexisted with a small residual amount of tetragonal−pyramidal O═MoO_4. The residual presence of tetragonal−pyramidal O═MoO_4 in the 973 K treated sample is consistent with the presence of weak bands at 652 and 814 cm^{-1} (spectrum g in Figure 10), which can be assigned to its symmetric and antisymmetric ν(O−Mo−O) modes, respectively.

Conclusions

Isolated tetrahedral MoO_4, two-dimensional polymolybdates, tetragonal−pyramidal O═MoO_4, and crystalline MoO_3 and $Zr(MoO_4)_2$ species were detected by Raman and X-ray absorption spectroscopies and by X-ray diffraction in MoO_x/ZrO_2 samples with 1−44 wt % MoO_3 after treatment in air at 393−973 K. The Mo surface density range in these samples ranged from 0.35 to 50 Mo/nm^2. For Mo surface densities below the polymolybdate monolayer values (∼5 Mo/nm^2), no crystalline MoO_3 or $Zr(MoO_4)_2$ were detected by these methods after thermal treatment at 393−973 K. The size of these two-dimensional polymolybdate domains increased with increasing Mo surface density; this process led to a shift in the ν(Mo═O) Raman band, to changes in the near-edge X-ray absorption spectra, and to a decrease in the UV−visible edge energy with increasing surface density. Domain growth occurred via oligomerization of isolated tetrahedral MoO_x as thermal treatments decreased the ZrO_2 surface area available to disperse the MoO_x species. This formation of Mo−O−Mo linkages was reversed at higher temperatures (973 K), which led to the dissociation on Mo−O−Mo bonds in polymolybdates and to the formation of tetragonal−pyramidal O═MoO_4 species. Crystalline MoO_3 and $Zr(MoO_4)_2$ were formed in samples with Mo surface densities above 5 Mo/nm^2. Treatment in air at temperatures below 873 K leads to the preferential formation of MoO_3, while higher temperatures favor the solid-state reaction between MoO_3 and ZrO_2 to form exclusively $Zr(MoO_4)_2$.

Acknowledgment. We acknowledge Dr. George D. Meitzner for his expert help in the acquisition and analysis of X-ray absorption data. This work was supported by the Director, Office of Basic Energy Sciences, Chemical Sciences Division of the U.S. Department of Energy (DOE) under Contract DE-AC03-76SF00098. X-ray absorption data were collected at the Stanford Synchrotron Radiation Laboratory (SSRL), which is operated by the Department of Energy, Office of Basic Energy Sciences.

References and Notes

(1) Albonetti, S.; Cavani, F.; Trifiro, R. *Catal. Rev.-Sci. Eng.* **1996**, *38*, 413 and references therein.
(2) Blasko, T.; Lopex Nieto, J. M. *Appl. Catal.* **1997**, *157*, 117.
(3) Kung, H. H. *Adv. Catal.* **1994**, *40*, 1.
(4) Cavani, F.; Trifiro, F. *Appl. Catal.* **1995**, *133*, 219.
(5) Mamedov, E. A.; Cortes-Corberan, V. *Appl. Catal.* **1995**, *127*, 1.
(6) Busca, G. *Catal. Today* **1996**, *27*, 457.
(7) Deo, G.; Wachs, I. E. *J. Phys. Chem.* **1991**, *95*, 5889.
(8) Centi, G.; Trifiro, F. *Appl. Catal. A: General* **1996**, *143*, 3.
(9) Michalakos, P.; Hung, M. C.; Jahan, I.; Kung, H. H. *J. Catal.* **1993**, *140*, 226.
(10) Khodakov, A.; Yang, J.; Su, S.; Iglesia, E.; Bell, A. T. *J. Catal.* **1998**, *177*, 343.
(11) Chen, K. D.; Xie, S.; Bell, A. T.; Iglesia, E. *J. Catal.* **2000**, *189*, 421.
(12) Stencel, J. M. *Raman Spectroscopy for Catalysis*; van Nostrand Reinhold: New York, 1990.
(13) Schrader, B., Ed. *Infrared and Raman Spectroscopy: Methods and Applications*; VCH: Weinheim, 1995.
(14) Mestl, G.; Srinivasan, T. K. K. *Catal. Rev.* **1998**, *40*, 451.
(15) Hardcastle, F. D.; Wachs, I. E. *J. Raman Spectrosc.* **1990**, *21*, 683.
(16) Meitzner, G. D. *Catal. Today* **1998**, *39*, 281.
(17) Barton, D. G. Ph.D. Thesis, University of California at Berkeley, 1998.
(18) Ressler, T. *J. Phys. IV* **1997**, *7*, 269.
(19) Ressler, T. *J. Synch. Rad.* **1998**, *5*, 118.
(20) Hillerová, E.; Morishige, H.; Inamura, K.; Zdrazil, M. *Appl. Catal. A: Gene.* **1997**, *156*, 1.
(21) Prinetto, F.; Cerrato, G.; Ghiotti, G.; Chiorino, A.; Campa, M. C.; Gazzoli, D.; Indovina, V. *J. Phys. Chem.* **1995**, *98*, 5556.
(22) Sonnemans, J.; Mars, P. *J. Catal.* **1973**, *31*, 209.
(23) Xie, Y.; Tang, Y. *Adv. Catal.* **1990**, *37*, 1.
(24) Wang, X.; Zhao, B.; Jiang, D.; Xie, Y. *Appl. Catal. A: Gene* **1999**, *188*, 201.
(25) Liu, Z.; Chen, Y. *J. Catal.* **1998**, *177*, 314.
(26) Liu, Z.; Dong, L.; Chen, Y. *J. Chem. Soc., Faraday Trans.* **1998**, *94*, 1137.
(27) Del Arco, M.; Carrazán, S. R. G.; Rives, V.; Gil-LlambRas, F. J.; Malet, P. *J. Catal.* **1993**, *141*, 48.
(28) Dufresne, P.; Payne, E.; Grimblot, J.; Bonnelle, J. P. *J. Phys. Chem.* **1981**, *85*, 5, 2344.
(29) Zingg, D. S.; Makovsky, L. E.; Tischer, R. E.; Brown, F. R.; Hercules, D. M. *J. Phys. Chem.* **1980**, *84*, 2898.
(30) Edwards, J. C.; Adams, R. D.; Ellis, P. D. *J. Am. Chem. Soc.* **1990**, *112*, 8349.
(31) Xie, S.; Iglesia, E.; Bell, A. T. *Chem. Mater.* **2000**, *12*, 2442.
(32) Etsell, T. H.; Flengas, S. N. *Chem. Rev.* **1970**, *70*, 339.
(33) Barton, D. G.; Soled, S. L.; Meitzner, G. D.; Fuentes, G. A.; Iglesia, E. *J. Catal.* **1999**, *181*, 57.
(34) Xie, S.; Iglesia, E.; Bell, A. T. Unpublished results.
(35) Auray, M.; Quarton, M.; Tarte, P. *Acta Crystallogr.* **1986**, *C42*, 257.
(36) Nakamoto, K. *Infrared and Raman Spectra of Inorganic and Coordination Compounds*, 4th ed.; John Wiley & Sons: New York, 1986; pp130−141.
(37) Herzberg, G.; *Molecular Spectra and Molecular Structure*; van Nostrand: New York, 1945.
(38) Weinstock, N.; Schulze, H.; Müller, A. *J. Chem. Phys.* **1973**, *59*, 5063.
(39) Li, W.; Meitzner; G. D.; Borry, R. W.; Iglesia, E. *J. Catal.* **2000**, *191*, 373.
(40) Shadle, E.; Hedman, B.; Hodgson, K. O.; Solomon, E. I. *Inorg. Chem.* **1994**, *33*, 4235.
(41) Vuurman, M. A.; Wachs, I. E. *J. Phys. Chem.* **1992**, *96*, 5008.
(42) Jeziorowski, H.; Knözinger, H. *J. Phys. Chem.* **1979**, *83*, 1166.
(43) Cheng, C. P.; Schrader, G. L. *J. Catal.* **1979**, *60*, 276.
(44) Wang, L.; Hall, W. K. *J. Catal.* **1980**, *66*, 251.
(45) Wachs, I. E. *Catal. Today* **1996**, *27*, 437.
(46) Chan, S. S.; Wachs, I. E.; Murrell, L. L.; Wang, L.; Hall, W. K. *J. Phys. Chem.* **1984**, *88*, 5831.
(47) Miyata, H.; Tokuda, S.; Ono, T.; Ohno, T.; Hatayama, F. *J. Chem. Soc. Faraday Trans.* **1990**, *86*, 2291.
(48) Payen, E.; Kasztelan, S.; Grimblot, J.; Bonnelle, J. P. *J. Raman Spectrosc.* **1986**, *17*, 233.
(49) Stencel, J. M.; Makovsky, L. E.; Sarkus, T. A.; de Vries, J.; Thomas, R.; Mouljin, J. A. *J. Catal.* **1984**, *90*, 314.
(50) Knözinger, H.; Jeziorowski, H. *J. Phys. Chem.* **1979**, *83*, 1166.
(51) Weber, R. S. *J. Catal.* **1995**, *151*, 470.
(52) Xiong, G.; Li, C.; Feng, Z.; Ying, P.; Xin, Q.; Liu, J. *J. Catal.* **1999**, *186*, 234.
(53) Collin, R. J.; Griffith, W. P.; Pawson, D. *J. Mol. Struct.* **1973**, *19*, 531.
(54) Alexander, L. E.; Beattie, I. R.; Bukovszky, A.; Jones, P. J.; Marsden, C. J.; van Schalkwyk, G. J. *J. Chem. Soc., Dalton Trans.* **1974**, 81.
(55) Paiine, R. T.; McDowell, R. S. *Inorg. Chem.* **1974**, *13*, 2366.
(56) Beatties, I. R.; Livingston, K. M. S.; Reynolds, D. J.; Ozin, G. A. *J. Chem. Soc. A* **1970**, 1210.
(57) Iijima, K.; Shibata, S. *Bull. Chem. Soc., Jpn.* **1975**, *48*, 666.
(58) Desikan, A. D.; Huang, L.; Oyama, S. T. *J. Chem. Soc., Faraday Trans.* **1992**, *88*, 3357.
(59) Mercera, P. D. L.; van Ommen, J. G.; Doesburg, E. B. M.; Burggraaf, A. J.; Ross, J. R. H. *Appl. Catal.* **1990**, *57*, 127.
(60) Murase, Y.; Kato, E. *J. Am. Ceram. Soc.* **1983**, *66*, 196.
(61) Ma, E. *Bull. Chem. Soc. Jpn.* **1964**, *37*, 648.
(62) Xie, S.; Bell, A. T.; Iglesia, E. Unpublished results.
(63) Aritani, H.; Tanaka, T.; Funabiki, T.; Yoshida, S.; Kudo, M.; Hasegawa, S. *J. Phys. Chem.* **1996**, *100*, 5440.
(64) Verbruggen, N. F. D.; Mestl, G.; von Hoppel, L. M. J.; Lengeler, B.; Knözinger, H. *Langmuir* **1994**, *10*, 3063.
(65) Takenaka, S.; Tanaka, T.; Funabiki, T.; Yoshida, S. *J. Phys. Chem. B* **1998**, *102*, 2960.